Thermal Evaporation Processing of Nano and Submicron Tin Oxide Rods

S. Shukla, V. Venkatachalapathy, and S. Seal*

Surface Engineering and Nanotechnology Facility (SNF), Advanced Materials Processing and Analysis Center (AMPAC), Engineering 381, University of Central Florida (UCF), Orlando, Florida 32816

Received: February 16, 2006; In Final Form: April 5, 2006

Nano and submicron rods of semiconductor tin oxide (SnO_2) have been synthesized via thermal evaporation technique. Various substrates such as oxidized silicon (Si/SiO_2), porous alumina (Al_2O_3), oxidized and anodized titanium (Ti/TiO_2), with the sputtered platinum (Pt) catalyst, have been utilized for this purpose. The effect of Pt sputtering time and the nature of the substrate on the size distribution and the morphology of the SnO_2 rods and their substrate-surface-coverage have been investigated. The formation of nano and submicron SnO_2 rods has been attributed to the vapor−liquid−solid (VLS) and vapor−solid (VS) growth mechanisms depending on the processing conditions.

Introduction

Tin oxide (SnO_2) is a well-known wide band gap (3.6 eV) n-type semiconductor, which is widely used for optoelectronic devices, transparent conductor, and gas sensor applications.[1−3] We are currently investigating the use of doped-tin oxide as a low-temperature hydrogen H_2 sensor.[4,5] Nanocrystalline doped-tin oxide thin films have been synthesized using the sol−gel technique and deposited over the microelectromechanical system (MEMS) device, which exhibited very high H_2 sensitivity (as high as 10^3-10^5) and selectivity over carbon monoxide (CO) at room temperature. The response time of the present SnO_2-based micro-sensor, however, lies in the range of 200−300 s at room temperature and needs to be reduced to few seconds for potential applications.

It has been recently reported that,[6] out of various morphologies of SnO_2, such as single nanowire, porous mesh of randomly oriented nanowires, and thin films, highest gas sensitivity is achieved using the thin film form of the sensor; however, minimum response time is exhibited only by the single nanowire form of the sensor. On the other hand, the porous mesh of randomly oriented SnO_2 nanowires is likely to give moderate gas sensitivity with reasonably lower detection time. Hence, much attention has been given to synthesize the randomly oriented porous structure of SnO_2 nanowires using different processing techniques.

In this report, we demonstrate the synthesis of nano and submicron SnO_2 rods via thermal evaporation technique. The synthesis of nanowires of SnO_2,[7−13] indium oxide (In_2O_3),[14−16] zinc oxide (ZnO),[17−21] titania (TiO_2),[22−24] and silica (SiO_2),[25−27] using thermal evaporation technique has been reported earlier in the literature. However, since the nano and submicron SnO_2 rods, in this investigation, have been synthesized for the fabrication of a gas sensor device in the near future, various substrates have been utilized to identify the one, which would give the maximum substrate-surface-coverage (qualitatively defined here as the surface area covered by the nano and submicron SnO_2 rods relative to the total surface area of the substrate) of SnO_2 rods with the minimum SnO_2 rod size. Attention has been given to analyze the different morphologies of the nano and submicron SnO_2 rods produced and the underlying growth mechanisms.

Experimental Section

(a) Chemicals and Substrates. Tin oxide (SnO) and indium (In) powders were supplied by Alfa Aesar, U.S.A. and used as received. Oxidized silicon wafers (Si/SiO_2) having 1 μm thick SiO_2 layer, pure titanium (Ti) foil having thickness 0.5 mm, and porous alumina (Al_2O_3) substrates having uniform pores of size 100 nm were supplied by Fischer Scientific Inc., U.S.A..

(b) Substrate Preparation. Small pieces having the surface area 1 cm × 1 cm were cut from the respective wafers or foils, then cleaned in 2-propanol using the ultrasonic cleaner, and then dried in an oven at 120 °C for 15 min. One of the Ti-substrate was heated in the furnace at 1000 °C, at a constant heating rate of 30 °C/min with the holding time of 12 h, to produce a thick TiO_2 layer (referred to as oxidized Ti/TiO_2). Another Ti-substrate was subjected to anodization treatment[28,29] to grow a nanoporous array of TiO_2 nanotubes on the surface (referred to as anodized Ti/TiO_2). All of the four substrates (oxidized Si/SiO_2, porous Al_2O_3, and oxidized and anodized Ti/TiO_2) were sputtered coated (K350, Emitech, Ashford, Kent, England) with a thin layer of platinum (Pt) for different time intervals, which has been specified in the following text as necessary.

(c) Thermal Evaporation Processing. Thoroughly mixed SnO (2.0 g) and In (0.24 g) powders were kept in Al_2O_3 boat, which was subsequently placed centered (where the thermocouples were located) in a horizontal Al_2O_3 tube (inner and outer diameters 3.2 and 3.5 in respectively and length 42 in) of a high-temperature furnace, Figure 1. All four substrates were also placed in the same Al_2O_3 boat, which contained the mixture of SnO and In powders. After inserting the precursor powder mixture and the substrates into the horizontal Al_2O_3 tube, both the ends of the tube were closed using mechanically clamped steel plates with the rubber gaskets. Flow of cooling water was started and maintained throughout the experiment to avoid overheating of the steel plates and the rubber gaskets. An internal fan, located inside the high-temperature furnace, was turned on to cool the external surface of the horizontal Al_2O_3 tube. Argon (Ar) gas was blown into the furnace at the speed of 70 scfm

* Corresponding author. Phone: (407) 882-1119. Fax: (407) 882-1462. E-mail: sseal@mail.ucf.edu.

10.1021/jp061009b CCC: $33.50
Published on Web 05/19/2006

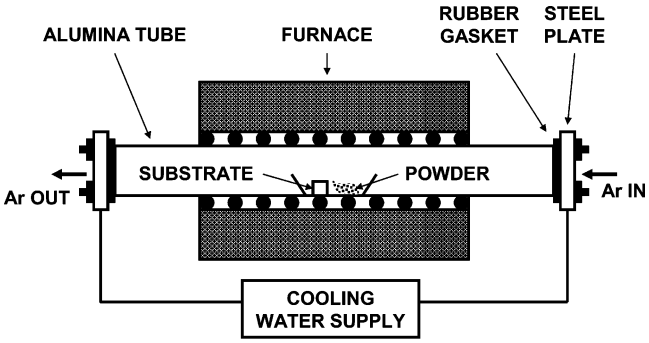

Figure 1. Schematic diagram describing the furnace setup used for growing the nano and submicron SnO_2 rods via thermal evaporation process.

(standard cubic feet per minute) for the first 10 min to completely displace the air within the horizontal Al_2O_3 tube. The Ar flow was then reduced to 20 scfm for the entire heating and cooling cycle; however, the flow was restored to 70 scfm for the last 10 min of the experiments. The high-temperature furnace was programmed for the heating and cooling cycles. The furnace was heated from room temperature to the processing temperature (800 °C or 900 °C) in 5 h, held at that temperature for 2 h, and then cooled to room temperature within the next 5 h. All thermal evaporation experiments were conducted at 760 Torr pressure. After the furnace had cooled to room temperature, the ends of the horizontal Al_2O_3 tube were opened by unclamping the steel plates and the substrates with the deposited nano and submicron SnO_2 rods were removed for further analysis.

(d) Characterization. The as-synthesized nano and submicron SnO_2 rods were sputtered coated with Pt layer for 4 min to avoid charging effects during the image analysis using the scanning electron microscope (JSM-6400F, JEOL, Tokyo, Japan). The SEM images at different magnifications were obtained to determine the average SnO_2 rod size (apparent diameter) and their morphologies under different processing conditions. Energy dispersive analysis of X-rays (EDX) was performed to determine the chemical constituents of the rods. The crystal structure of the SnO_2 rods was determined using the X-ray diffraction (XRD, Rigaku, Japan) using the Cu $K\alpha$ radiation (wavelength = 1.54 Å).

Results

(a) Si/SiO_2 Substrate. Typical SEM images of the as-synthesized SnO_2 rods deposited on the Si/SiO_2 substrates at the processing temperature of 900 °C are presented in Figure 2. In Figures 2a,c, the Pt sputtering time is increased as 30 s, 60 s, and 120 s respectively, which effectively varies the Pt catalyst size at the evaporation temperature. Randomly oriented, straight and long rods, as long as 50 μm, are formed under these processing conditions. It is noted that, the apparent diameter of the rod is a function of the Pt sputtering time. In Figures 2a,c, the rod size distribution (which is determined using the high magnification images and measuring the minimum and the maximum rod size) lies within the range of 100−400 nm, 200−700 nm, and 600−1000 nm, respectively. The rod size is, thus, noted to increase with increasing Pt sputtering time within the range of 30−120 s. As shown in the inset in Figure 2c, the rods have a hexagonal cross-section. It is also noted that, the catalyst particles located at the tip of the rods are not observed in Figure 2.

Moreover, the SnO_2 rods are observed to form only for the Pt sputtering time of less than 120 s; with increasing Pt sputtering time above 120 s, only the formation of thin films of SnO_2 nanoparticles has been noted. Although, the substrate-surface-coverage of nano and submicron SnO_2 rods increases with decreasing Pt sputtering time, the overall coverage over Si/SiO_2 substrate was relatively smaller.

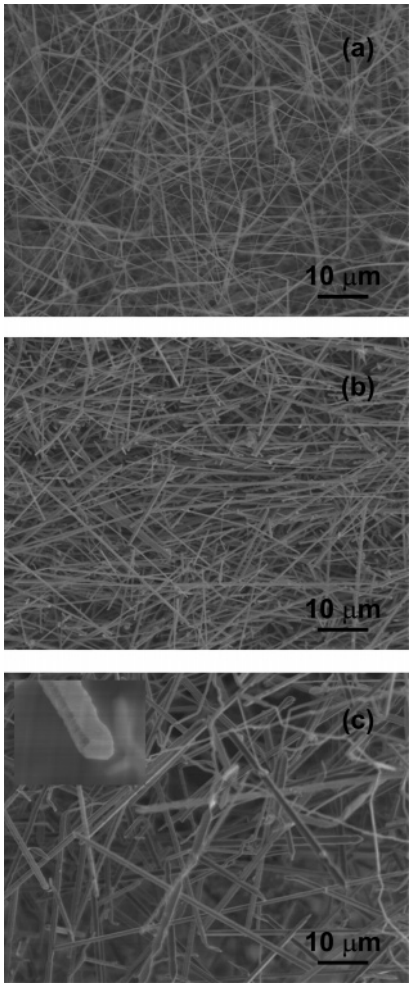

Figure 2. SEM images of nano and submicron SnO_2 rods grown, at the processing temperature of 900 °C, on the Pt-sputtered Si/SiO_2 substrate. The Pt sputtering time is varied as (a) 30 s, (b) 60 s, and (c) 120 s. No catalyst particle located at the tip of the rod is noted. An inset in (c) shows the hexagonal cross-section of the SnO_2 rod.

Although rods having hexagonal cross-section with no catalyst particles at the tip were observed using the Si/SiO_2 substrate, the formation of other morphology of the as-synthesized SnO_2 rods was also noticed (for Pt sputtering time of 30 s) and is presented in Figure 3 at different magnifications. These randomly oriented SnO_2 rods appear to be shorter in length than those presented in Figure 2a. In contrast to the morphology of SnO_2 rods presented in Figure 2a, the second morphology as observed in Figure 3, does exhibit the presence of a catalyst particle at the tip of each rod, thus, giving a "pin-like" morphology. The size of the catalyst particle appears to be larger than the rod size. The SnO_2 rods shown in Figure 3 are relatively more vertical (defined here as the orientation of the SnO_2 rods relative to the substrate-surface, which is parallel to the plane of the SEM images) than those presented in Figure 2a. The rod size is noted be within the range of 300−600 nm. Moreover, the rods with the catalyst particle at the tip also have a noncircular cross-section similar to that shown in the inset of Figure 2c.

The EDX analysis of the rods synthesized using the Pt sputtering time of 30 s is presented in Figure 4a. The EDX

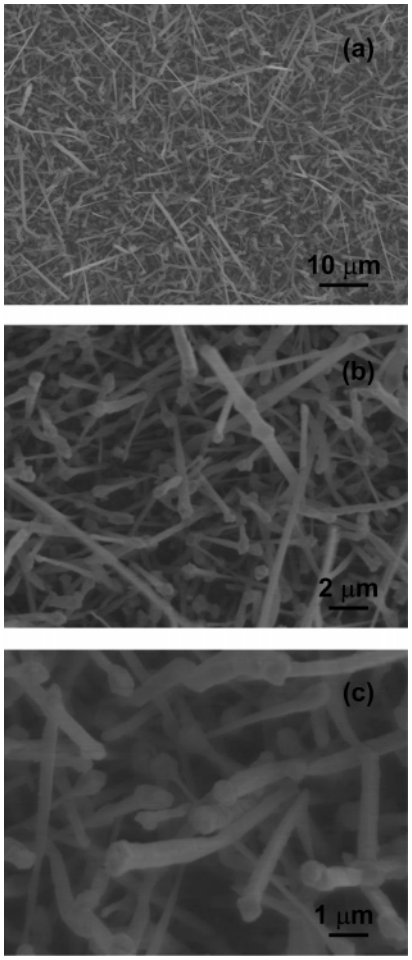

Figure 3. SEM images, at different magnifications, of nano and submicron SnO_2 rods having "pin-like" morphology, grown at the processing temperature of 900 °C, on the Pt-sputtered (30 s) Si/SiO_2 substrate. A catalyst particle located at the tip of the rod is noted.

spectrum shows the presence of Sn, O, and Pt as the major constituents within the rods. The Sn and O within the rods originate from the precursor powders utilized during the thermal evaporation processing and suggests the formation of nano and submicron SnO_2 rods; while the Pt peak originates either from the Pt catalyst or the Pt sputtered thin film (which avoids the charging effect during the SEM image analysis). The presence of In within the SnO_2 rods is, however, not distinctly noted in the EDX spectrum due to the very close proximity of In- and Sn-peaks.

The broad scan XRD spectrum within the 2-θ range of 10−80°, obtained using the rods synthesized using the Pt sputtering time of 30 s, is presented in Figure 4b. The presence of the XRD pattern suggests the crystalline nature of the as-synthesized rods and their crystal structure appears to be tetragonal−SnO_2 (cassiterite) as per the JCPDS card no. 41-1445. The EDX and the XRD spectra obtained using the SnO_2 rods synthesized under different processing conditions are similar to those presented in Figure 4, which confirms the formation of nano and submicron SnO_2 rods.

(b) Porous Al_2O_3 Substrate. The SEM images of the as-synthesized nano and submicron SnO_2 rods grown on the Pt-sputtered (30 s) porous Al_2O_3 substrates (pore size: 100 nm) at the processing temperature of 900 °C are presented in Figure 5 at different magnifications. The substrate-surface-coverage of the nano and submicron SnO_2 rods on the porous Al_2O_3 substrate has been limited similar to the previous case of Pt-sputtered

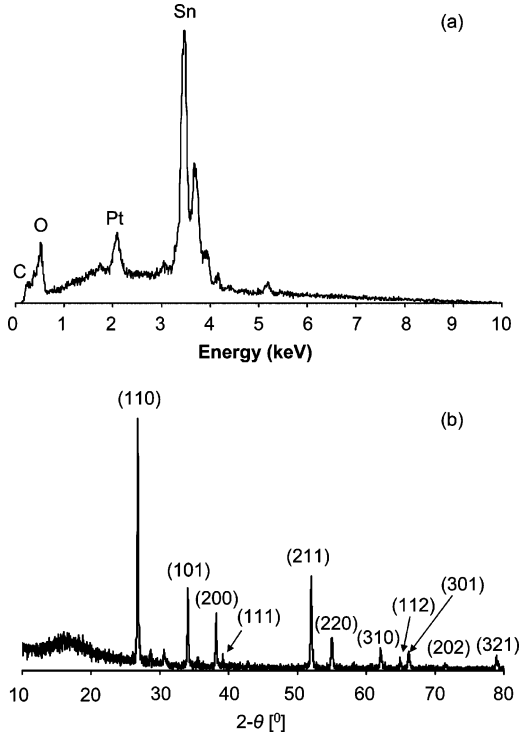

Figure 4. EDX (a) and XRD (b) spectra obtained using the nano and submicron SnO_2 rods, grown at the processing temperature of 900 °C, on the Pt-sputtered (30 s) Si/SiO_2 substrate.

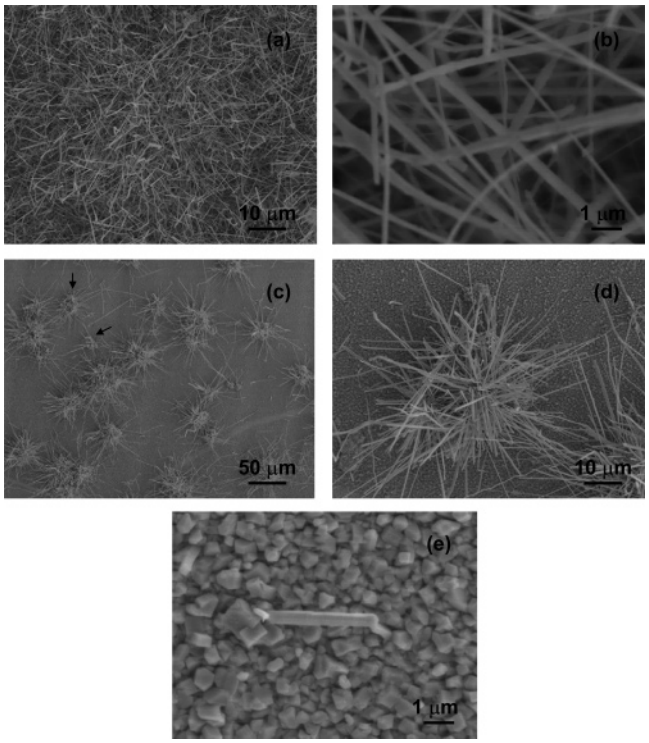

Figure 5. SEM images of nano and submicron SnO_2 rods grown, at the processing temperature of 900 °C, on the Pt-sputtered (30 s) porous Al_2O_3 substrate. Different SnO_2 morphologies can be noted: (a−b) randomly oriented rods with no catalyst particle located at the tip, and (c−d) "asterisk-like" structure, under the background of thin film of SnO_2 nanoparticles, without a catalyst particle located at the tip of the rod. In (e), a single submicron SnO_2 rod growing from the thin film of faceted SnO_2 nanoparticles is seen.

Si/SiO_2 substrate. Two different types of SnO_2 rod morphologies have been observed as shown in Figure 5. In Figures 5a,b,

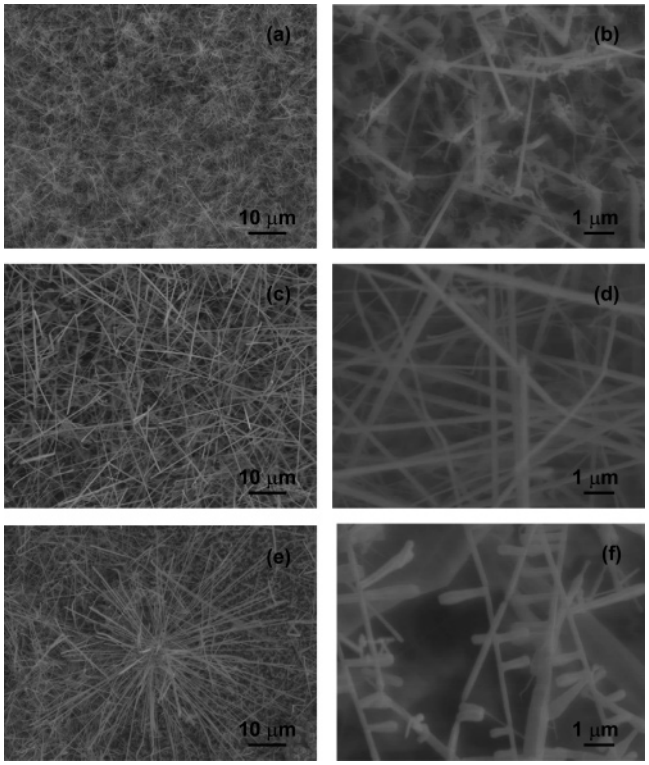

Figure 6. SEM images of nano and submicron SnO_2 rods grown, at the processing temperature of 900 °C, on the Pt-sputtered (30 s) oxidized Ti/TiO_2 substrate. Different SnO_2 morphologies have been noted: (a−b) randomly oriented short rods with and without the catalyst particle at the tip, (c−d) randomly oriented long rods with no catalyst particle located at the tip, (e) an "asterisk-like" structure, under the background of randomly oriented short SnO_2 rods, without a catalyst particle at the tip, and (f) a "dendritic-like" structure.

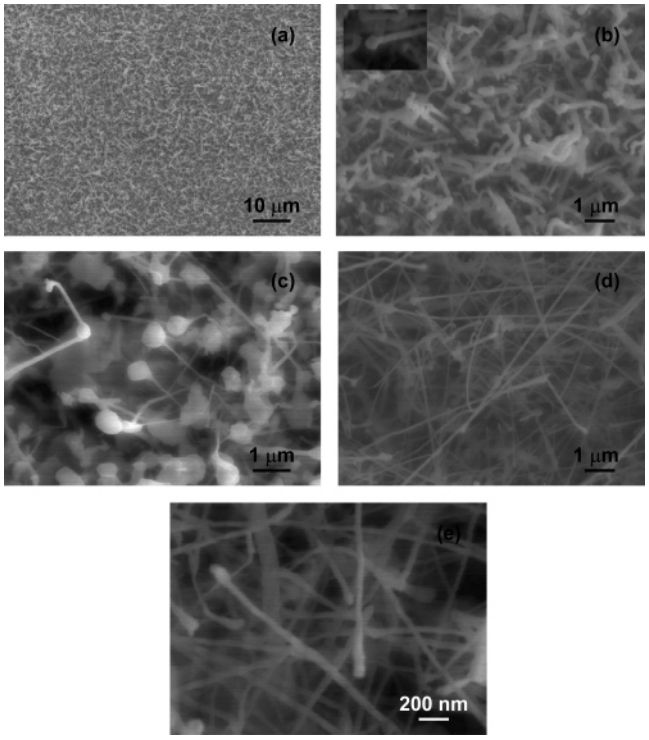

Figure 7. SEM images of nano and submicron SnO_2 rods grown, at the processing temperature of 800 °C, on the Pt-sputtered (30 s) anodized Ti/TiO_2 substrate. Different SnO_2 morphologies have been noted: (a−c) randomly oriented short rods with the catalyst particle located at the tip, (d−e) randomly oriented SnO_2 rods with the catalyst particle located at the tip. An inset in (b) shows the SnO_2 rod with a catalyst particle at the tip.

randomly oriented, long and straight SnO_2 rods, as long as 12 μm, are observed. The length of the SnO_2 rods is, thus, noted to be relatively shorter than that observed in Figure 2a. The SnO_2 rod size is observed to vary within the range of 60−450 nm, which is, however, comparable with that observed in Figure 2a. Moreover, no catalyst particle located at the tip of the SnO_2 rod is observed.

As shown in Figures 5c,d, a second morphology consisting "asterisk-like" growth of nano and submicron SnO_2 rods is seen at several different locations on the surface of Pt-sputtered porous Al_2O_3 substrate. These locations with the "asterisk-like" structure were slightly away from the regions with long and straight SnO_2 rods. Such a growth pattern is typically observed under the background of the thin film of SnO_2 nanoparticles. As shown by arrows in Figure 5c, the SnO_2 rods originating from the big size SnO_2 particles have been noted. It appears that, a big size SnO_2 particle, located at the center of the "asterisk-like" structure in Figure 5d, has been concealed by the presence of large number of SnO_2 rods. Further away from the region with the asterisk-like growth, an inclined single SnO_2 rod, without a catalyst particle at the tip, is noticed, which appears to be growing from the deposited thin film of SnO_2 nanoparticles.

(c) Oxidized Ti/TiO_2 Substrate. The SEM images of nano and submicron SnO_2 rods grown on the surface of the Pt-sputtered (30 s) oxidized Ti/TiO_2 substrate, at the processing temperature of 900 °C, are presented in Figure 6. Four different morphologies of the SnO_2 rods are observed in Figure 6. In Figures 6a,b, randomly oriented short (less than 6 μm in length) SnO_2 rods are seen. The rod size is measured to lie within the range of 30−200 nm, which is relatively smaller than that observed using the Pt-sputtered Si/SiO_2 and porous Al_2O_3 substrates. It appears in this case that the SnO_2 rods, with and without the catalyst particle at the tip, are grown simultaneously in one region, Figure 6b.

In Figures 6c,d, the second morphology of nano and submicron SnO_2 rods, observed on the surface of oxidized Ti/TiO_2 substrate, is shown. Randomly oriented, long and straight SnO_2 rods, as long as 35 μm, are observed in Figure 6c; while the rod size lies within the range 60−300 nm, which is smaller than those observed for the Pt-sputtered Si/SiO_2 and porous Al_2O_3 substrates.

The SnO_2 rods forming the asterisk-like structure, similar to those observed in Figures 5c,d, are also noted for the Pt-sputtered oxidized Ti/TiO_2 substrate, Figure 6d. However, as compared to the previous substrate, very few asterisk-like structures are formed in the present case. Moreover, this asterisk-like structure is noted to form under the background of the short and randomly oriented SnO_2 rods, Figure 6a. The forth morphology, consisting a "dendritic-like" structure of the SnO_2 rods is shown in Figure 6e. It appears that, the SnO_2 rods as long as 8 μm form the main branch in the dendritic-like structure; several short rods with length 1−2 μm are seen to grow as the secondary branches almost in the perpendicular direction to the main branch. The size of the secondary branches is noted to increase with increasing distance from the main branch. In addition to this, the size of the secondary branches is larger than that of the main branch.

(d) Anodized Ti/TiO_2 Substrate. Three different types of morphologies of nano and submicron SnO_2 rods grown on the Pt-sputtered (30 s) anodized Ti/TiO_2 substrate, at the processing temperature of 800 °C, are presented in Figure 7 (note: the

TABLE 1: Summary of Types of Substrates, Processing Conditions, and the Resulting Morphologies and Size Range of Thermal Evaporation Processed Nano and Submicron SnO_2 Rods

substrate	Pt sputtering time (sec)	processing temperature (°C)	morphology of SnO_2 nano and submicron rods	apparent rod diameter (nm)
Si/SiO_2	30	900	randomly oriented and long	100−400
			pin-like, catalyst particle at Tip	300−600
	60	900	randomly oriented and long	200−700
	120	900		600−1000
porous Al_2O_3	30	900	randomly oriented and long asterisk-like	60−450
oxidized Ti/TiO_2	30	900	randomly oriented and short, with and without catalyst particle at tip	30−200
			randomly oriented and long asterisk-like dendritic-like	60−300
anodized Ti/TiO_2	30	800	randomly oriented and short, catalyst particle at tip	100−300
			short, big Size catalyst particle at tip	600 (catalyst size) 50 (minimum rod size)
			randomly oriented and long, with and without catalyst particle at tip	60−150

nano and submicron SnO_2 rods are synthesized at slightly lower processing temperature than that used in the previous cases). In Figures 7a,b, randomly oriented, short SnO_2 rods, having a length less than 2 μm and size within the range of 100−300 nm, are visible. The presence of a catalyst particle at the tip of the SnO_2 rods is seen in the image of one of the SnO_2 rods, as shown in the inset in Figure 7b. The second morphology of the SnO_2 rods, observed on the surface of the Pt-sputtered anodized Ti/TiO_2 substrate, is shown in Figure 7c. The presence of a big size (600 nm) catalyst particle at the tip of SnO_2 rods is clearly visible. It further appears that, the size of SnO_2 rods is as small as 50 nm, which supports the large catalyst particle at the tip. The third morphology, consisting randomly oriented long and straight SnO_2 rods, is presented in Figure 7d, where the SnO_2 rods as long as 10 μm are observed with the size in the range of 60−150 nm. The SnO_2 rods with and without the catalyst particle at the tip are observed in Figure 7d. At higher magnification, Figure 7e, the SnO_2 rod size as small as 12 nm has also been noted. It appears that, the SnO_2 rod size is the smallest in this case possibly due to the lower processing temperature (800 °C).

Discussion

In the present investigation, nano and submicron SnO_2 rods have been synthesized using the thermal evaporation process using four different substrates and two different processing temperatures (800 and 900 °C). It is necessary to distinguish here between the terms "fibers" and "rods" as one may regard the SnO_2 rods synthesized in this investigation as SnO_2 fibers. The fibers are, in general, curved or flexible in contrast to the rigid or straight morphology of the rods. The synthesis of SnO_2 fibers via electrospinning technique by using the polymer fibers as templates has been demonstrated recently.[30] In contrast to the curved or flexible morphology of the electrospun SnO_2 fibers, the rigid or straight morphology observed in this investigation, suggests the synthesis of nano and submicron SnO_2 rods via thermal evaporation process. A summary of different morphologies of nano and submicron SnO_2 rods obtained under different processing conditions is provided in Table 1.

In the presence of a catalyst particle, such as Pt, the nucleation and growth of the SnO_2 rods via thermal evaporation process take place via vapor−liquid−solid (VLS) mechanism.[31,32] In this mechanism, the following chemical reactions are likely to occur at the operating temperature of 800 and 900 °C:[9,13]

$$2SnO_{(s)} \rightarrow Sn_{(l)} + SnO_{2(s)} \quad (1)$$

$$In_{(s)} \rightarrow In_{(l)} \quad (2)$$

The addition of In powder to the SnO powder is beneficial as the liquid In may alloy with liquid Sn; thus, reducing its melting temperature, which in turn, may increase the evaporation rate of Sn atoms at the processing temperature.

$$Sn_{(l)} \rightarrow Sn_{(v)} \quad (3)$$

Moreover, since the thermal evaporation process has been conducted in the Ar atmosphere at 760 Torr pressure, the lower oxygen partial pressure thus created is conducive for the decomposition of SnO_2, which is produced via reaction-1:

$$SnO_{2(s)} \rightarrow SnO_{(s)} + {}^1/_2O_{2(g)} \quad (4)$$

The Sn and O atoms in the vapor forms, formed via reactions 3 and 4, are then transported to the substrates, which are presputtered with a thin film of Pt. This amorphous Pt thin film, sputtered at room temperature, gets converted into the dispersed Pt nanocrystalline particles when the temperature is ramped from the room temperature to the processing temperature (800 or 900 °C). After coming in contact with the substrate having the dispersed Pt nanocrystalline particles, the Sn and O atoms, carried by the Ar gas, may get dissolved into the Pt nanoparticles forming Pt−Sn−O catalyst nanoparticles, which may result in the melting of the initial solid Pt nanoparticles. After reaching the solubility limit, further dissolution of Sn and O atoms from the vapor phase into the liquid Pt−Sn−O nanoparticles, results in the phase separation in the form of precipitation of SnO_2 nanorods. Being in the molten state, the Sn-rich Pt−Sn−O catalyst nanoparticles remain on the top of the precipitated SnO_2 rods. The molten Pt−Sn−O catalyst particle, possibly solidifies as the furnace cools below the melting temperature of the catalyst particle. This VLS growth mechanism should then result in the formation of SnO_2 rod with a catalyst particle at its tip.[12,13] Such morphology has been typically noted in the present investigation for the nano and submicron SnO_2 rods grown on

the Pt-sputtered Si/SiO_2 (Figure 3), oxidized (Figure 6b) and anodized Ti/TiO_2 substrates (Figure 7b,c).

In the present investigation, the nano and submicron SnO_2 rods are also formed without a catalyst particle at the tip. In this situation, the formation of SnO_2 rods does not take place via VLS mechanism but through the vapor−solid (VS) mechanism (alternatively known as "oxide-assisted-growth" mechanism).[12] In this mechanism, the initial Pt-catalyst particle assists in the formation of a thin film of faceted SnO_2 nanoparticles. These SnO_2 nanoparticles then act as nuclei for the growth of the SnO_2 nanorods via direct deposition of Sn and O atoms from the vapor phase on their surfaces, as is evident in Figure 5e. The growth of the nano and submicron SnO_2 rods via VS mechanism has been observed here for the Pt-sputtered Si/SiO_2 (Figure 2), porous Al_2O_3 (Figure 5), and oxidized Ti/TiO_2 substrates (Figures 6c and 6d). Thus, in the present investigation, both the VLS and the VS growth mechanisms are operative in the formation of nano and submicron SnO_2 rods on different Pt sputtered substrates.

As summarized in Table 1, different morphologies have been observed on different substrates, which possibly suggest that these substrates experience either VLS or VS or a combination of these mechanisms during the growth of nano and submicron SnO_2 rods. It is noted from Figures 2 and 3 that, for Si/SiO_2 substrate, the Pt sputtering time do govern the mechanism(s) of growth of SnO_2 rods. For the lower Pt sputtering time, both VLS and VS mechanisms are operative as the formation of nano and submicron SnO_2 rods, with and without the catalyst particle at the rod tip, has been observed. However, with increasing Pt sputtering time, only the VS mechanism becomes a dominant growth mechanism. Since, the Pt sputtering time may affect the Pt nanoparticle size distribution at the processing temperature, it appears that, the mechanism(s) responsible for the growth of SnO_2 rods may be a function of Pt nanoparticle size distribution at the processing temperature. Since, the surface diffusion coefficient for Pt may be different on the surfaces of different substrates, the Pt nanoparticle size distribution may be different on these substrates at the same processing temperature. Hence, we hypothesize that, different morphologies of nano and submicron SnO_2 rods produced on different substrates may be possibly due to the differences in the Pt nanoparticle size distribution at the same processing temperature.

It is also observed in the present investigation that, the different morphologies of nano and submicron SnO_2 rods, may or may not be present as physically mixed layers on the same substrate. This can also be explained on the basis of Pt nanoparticle size distribution at the processing temperature. Since, the Pt nanoparticles of different sizes would be distributed throughout the surface area of the same substrate, both VLS and VS growth mechanisms may be operative simultaneously in the adjacent regions resulting in the mixed morphologies of the SnO_2 rods.

It is further noted that, the Pt sputtering time (which, in turn, governs the average Pt nanoparticle size at the processing temperature) affects the size of the SnO_2 rods grown via VS mechanism and their substrate-surface-coverage (Figure 2). The increase in the size of the SnO_2 rods with increasing Pt sputtering time is possibly due to the formation of large size Pt nanoparticles (which subsequently act as catalyst particles for the growth of SnO_2 rods) with increasing sputtering time. Larger catalyst nanoparticle size is also observed to reduce the surface-coverage of the nano and submicron SnO_2 rods. It is also noted here that, the SnO_2 rods are formed on the Si/SiO_2 substrate, only when the Pt sputtering time is less than 120 s. Above this Pt sputtering time, only the formation of a thin film of faceted SnO_2 nanoparticles has been observed. Below the sputtering time of 120 s, the SnO_2 rod size decreases and the surface-coverage increases relatively. The maximum (or full) substrate-surface-coverage has been observed on the oxidized and the anodized Ti/TiO_2 substrates, while limited surface-coverage has been noted on Si/SiO_2 and porous Al_2O_3 substrates. As a result, from the application point of view (for example, fabrication of gas sensor devices[4,5]), the oxidized and the anodized Ti/TiO_2 substrates appear to be the best for the device manufacturing.

Further, the "asterisk-like" structure of SnO_2 rods, observed in this investigation, appears to be similar to the "cacti-like" morphology of ZnO nanowires as reported by others.[18] The cacti-like morphology of ZnO nanorods produced via thermal evaporation process has been attributed to the VLS growth mechanism. However, since the asterisk-like morphology of the SnO_2 nanorods has been observed under the background of the thin film of faceted SnO_2 nanoparticles (Figures 5c,d) or SnO_2 rods (Figure 6e), it appears that, the formation of such structure is related to the VS mechanism and not with the VLS mechanism. Earlier report has shown that, the cacti-like structure always consists of a big size particle at the center of the structure (that is, at the bottom of the nanorods).[18] In the present investigation, the big size SnO_2 nanoparticles, which are in the process of forming the asterisk-like structure around them, have been indicated by arrows in Figure 5c. The absence of the catalyst particle at the tip of individual SnO_2 rods within the asterisk-like morphology further supports the argument that these structures are formed via VS mechanism.

A dendritic form of the nanorod growth has also been noted in the present investigation for the oxidized Ti/TiO_2 substrate. Such form of growth has been reported earlier for SnO_2.[13] In this earlier report, the sub-branches within the dendritic structure are noted to be smaller in diameter relative to the size of the main branch. Moreover, the sub-branches have been observed to possess the ball-like particle at the tip, which suggest the growth of the sub-branches by VLS mechanism. In contrast to this, in the present investigation, the sub-branches are bigger in size relative to the size of the main branch (Figure 6f), while no ball-like feature is present at the tip of sub-branches; although the sub-branches increase in the size as they grow away from the main branch. These features possibly suggest that, in the present investigation, the sub-branches within the dendritic structure are grown via VS mechanism rather than the VLS mechanism. The underlying physical growth mechanisms for the formation of asterisk-like and dendritic-like morphologies are, however, not yet clearly understood; but, it has been proposed that they are related to the epitaxial growth process and the prevalence of habit (growth) planes.[33,34]

Last, we do observe the effect of processing temperature on the dimensions and the morphology of SnO_2 rods (although for two different substrates). By lowering the processing temperature by 100 °C, both the SnO_2 rod size and the rod length are effectively reduced, which may be beneficial for the gas sensing application. Moreover, since the lower processing temperature may reduce the Pt nanoparticle size distribution, VLS mechanism is likely to be a dominant growth mechanism relative to VS mechanism at lower processing temperature. This is possibly reflected in the absence of both asterisk-like and dendritic-like growth of nano and submicron SnO_2 rods at lower processing temperature.

Conclusions

(1) Nano and submicron SnO_2 rods have been synthesized via thermal evaporation technique using the Pt-sputtered Si/SiO_2, porous Al_2O_3, oxidized and anodized Ti/TiO_2 substrates.

(2) Various morphologies of nano and submicron SnO_2 rods such as pin, asterisk, and dendritic have been observed in the present investigation. The formation of pin-like morphology has been attributed to the VLS growth mechanism, while that of the asterisk-like and the dendritic-like structures has been ascribed to the VS growth mechanism.

(3) The size (apparent diameter) of the SnO_2 rods and their substrate-surface-coverage on the Pt-sputtered Si/SiO_2 substrate are the functions of the Pt sputtering time (that is, average size of the Pt nanoparticles at the processing temperature). The size of the SnO_2 rod increases and their substrate-surface-coverage decreases with increasing Pt sputtering time. Above the Pt sputtering time of 120 s, the nano and submicron SnO_2 rods are not obtained; only the formation of thin film of faceted SnO_2 nanoparticles is observed.

(4) The size of the nano and submicron SnO_2 rods lie within the range of 100−400 nm, 60−450 nm, 30−200 nm, and 60−150 nm for the Pt-sputtered (30 s) Si/SiO_2, porous Al_2O_3, oxidized and anodized Ti/TiO_2 substrates, respectively. Minimum SnO_2 rod size with maximum (or full) substrate-surface-coverage has been obtained for the oxidized and the anodized Ti/TiO_2 substrates, which make them suitable for the device fabrication.

Acknowledgment. We thank UCF, Florida Space Grant Consortium (FSGC), NASA-Glenn (NASA NAG 32751), KSC-NASA, and the National Science Foundation (NSF EEC-0136710 and NSF CTS 0350572) for funding the nanotechnology and the sensor research.

References and Notes

(1) Arnold, M. S.; Avouris, P.; Pan, Z. W.; Wang, Z. L. *J. Phys. Chem. B* **2003**, 107, 659.

(2) Chopra, K. L.; Major, S.; Pandya, D. K. *Thin Solid Films* **1982**, *102*, 1.

(3) Ding, J.; McAvoy, T. J.; Cavicchi, R. E.; Semancik, S.; *Sens. Actuators, B* **2001**, *77*, 597.

(4) Shukla, S.; Ludwig, L.; Cho, H. J.; Drake, C.; Seal, S. *J. Appl. Phys.* **2005**, *98*, 104306.

(5) Shukla, S.; Agrawal, R.; Ludwig, L.; Cho, H. J.; Seal, S. *J. Appl. Phys.* **2005**, *97*, 054307.

(6) Meyyappan, M.; Shukla, S.; Seal, S. *Interface* **2005**, *14*, 41.

(7) Calestani, D.; Zha, M.; Salviati, G.; Lazzarini, L.; Zanotti, L.; Comini, E.; Sberveglieri, G. *J. Cryst. Growth* **2005**, *275*, e2083.

(8) Ramgir, N. S.; Mulla, I. S.; Vijaymohanan, K. P. *J. Phys. Chem. B* **2005**, *109*, 12297.

(9) Cai, D.; Su, Y.; Chen, Y.; Jiang, J.; He, Z.; Chen, L. *Mater. Lett.* **2005**, *59*, 1984.

(10) Wang, Y.; Lee, J. Y.; Deivaraj, C. *J. Phys. Chem. B* **2004**, *108*, 13589.

(11) Ramgir, N. S.; Mulla, I. S.; Vijaymohanan, K. P. *J. Phys. Chem. B* **2004**, *108*, 14815.

(12) Zhang, R.-Q.; Lifshitz, Y.; Lee, S.-T. *Adv. Mater.* **2003**, *15*, 635.

(13) Dai, Z. R.; Pan, Z. L.; Wang, Z. L. *Adv. Funct. Mater.* **2003**, *13*, 9.

(14) Li, S. Y.; Lee, C. Y.; Lin, P.; Tseng, T. Y. *Nanotechnol.* **2005**, *16*, 451.

(15) Chen, Y. Q.; Jiang, J.; Wang, B.; Hou, J. G. *J. Phys. D. Appl. Phys.* **2004**, *37*, 3319.

(16) Liang, C.; Meng, G.; Lei, Y.; Phillip, F.; Zhang, L. *Adv. Mater.* **2001**, *13*, 1330.

(17) Bae, S. Y.; Na, C. W.; Kang, N. J.; Park, J. *J. Phys. Chem. B* **2005**, *109*, 2526.

(18) Xing, Y. J.; Xi, Z. H.; Zhang, X. D.; Song, J. H.; Wang, R. M.; Xu, J.; Xue, Z. Q.; Yu, D. P. *Appl. Phys. A* **2005**, *80*, 1527.

(19) Gao, P. X.; Zhong, L. W. *J. Phys. Chem. B* **2004**, *108*, 7534.

(20) Ding, Y.; Gao, P. X.; Wang Z. L. *J. Am. Chem. Soc.* **2004**, *126*, 2066.

(21) Yang, P.; Yan, H.; Mao, S.; Russo, R.; Jonhnson, J.; Saykally, R.; Morris, N.; Pham, J.; He, R.;, Choi, H.-J., *Adv. Funct. Mater.* **2002**, *12*, 323.

(22) Wu, J.-M.; Shih, H. C.; Wu, W.-T. *Chem. Phys. Lett.* **2005**, *413*, 490.

(23) Wu, J.-M.; Shih, H. C.; Wu, W.-T.; Tseng, Y.-K.; Chen, I.-C. *J. Crys. Growth* **2005**, *281*, 384.

(24) Wu, J.-M.; Shih, H. C.; Wu, W.-T. *Chem. Phys. Lett.* **2005**, *413*, 490.

(25) Noda, T.; Suzuki, H.; Araki, H.; Yang, W.; Shi, Y.; Tosa, M. *Appl. Surf. Sci.* **2005**, *241*, 231.

(26) Kolb, F. M.; Hofmeister, H.; Zacharias, M.; Gosele, U. *Appl. Phys. A* **2005**, *80*, 1405.

(27) Pan, Z. W.; Dai, Z. R.; Xu, L.; Lee, S. T.; Wang, Z. L. *J. Phys. Chem.* **2001**, *105*, 2507.

(28) Varghese, O. K.; Gong, D.; Paulose, M.; Ong, K. G.; Dickey, E. C.; Grimes, C. A. *Adv. Mater.* **2003**, *15*, 624.

(29) Gong, D.; Grimes, C. A.; Varghese, O. K.; Hu, W.; Singh, R. S.; Chen, Z.; Dickey, E. C. *J. Mater. Res.* **2001**, *16*, 3331.

(30) Shukla, S.; Brinley, E.; Cho, H. J.; Seal, S. *Polymer* **2005**, *46*, 12130.

(31) Wagner, R. S.; Ellis, W. C. *Appl. Phys. Lett.* **1964**, *4*, 889.

(32) Wu, Y.; Yan, H.; Huang, M.; Messer, B.; Song, J. H.; Yang, P. *Chem. Eur. J.* **2002**, *8*, 1261.

(33) Fan, H. J.; Scholz, R.; Kolb, F. M.; Zacharias, M. *Appl. Phys. Lett.* **2004**, *85*, 4142.

(34) Fan, H. J.; Scholz, R.; Kolb, F. M.; Zacharias, M.; Gosele U.; Heyroth, F.; Eisenschmidt, C.; Hempel, T.; Christen, J. *Appl. Phys. A* **2004**, *79*, 1895.